Supporting Information.

α-Synuclein induces both positive mean curvature and negative Gaussian curvature in membranes

Anthony R. Braun[1], Eva Sevcsik[2], Pamela Chin[3],

Elizabeth Rhoades[2], Stephanie Tristram-Nagle[4], and Jonathan N. Sachs[1*].

[1]Department of Biomedical Engineering, University of Minnesota, Minneapolis, MN 55455,

[2]Department of Molecular Biophysics and Biochemistry, Yale University, New Haven, CT 06520, and

[3]Douglass College, Rutgers University, New Brunswick, NJ 08901 and

[4] Department of Physics, Carnegie Mellon University, Pittsburgh, PA 15213.

Protein expression and purification

Plasmid encoding wild-type α-Synuclein (αS) was provided by David Eliezer at Weill Medical College of Cornell University and was used to generate our truncated αS (residues 1-100). The proteins are recombinantly expressed in E. coli and purified via ammonium sulfate precipitation, followed by ion exchange and size-exclusion chromatography, as previously published for full-length αS[3], modified by replacing the anion exchange column at pH 8.0 with a cation exchange column at pH 4.0. Purity of all the protein samples is verified by gel electrophoresis and mass spectrometry (generally, purity is >99%).

Protein labeling

For fluorescence correlation spectroscopy (FCS) experiments, αS was labeled with Alexa Fluor 488 maleimide (AL488) (Invitrogen, Carlsbad, CA) at cysteine introduced at residue 9 in Tris buffer (20 mM Tris, 130 mM NaCl, pH 7.4). UV-Vis absorbance at 495 nm was used to quantify the AL488 concentration, but was insufficiently sensitive for determination of αS concentration due to the large absorbance of AL488 (ε=7800 $M^{-1}cm^{-1}$) and the lower absorbance of αS (ε=5120 $M^{-1}cm^{-1}$) at 280 nm. The final protein concentration was determined by a modified Lowry assay (Bio-Rad, Hercules, CA). Labeling efficiencies were consistently between 85 and 95%.

Fluorescence correlation spectroscopy

FCS measurements were made on a lab-built instrument based around an Olympus IX71 inverted microscope and a 488 nm DPSS laser as described previously[3]. Laser power was adjusted to 5 μW prior to entering the microscope. Fluorescence emission was collected through the objective and separated from laser excitation

using a Z488rdc long pass dichroic and an HQ600/200m band-pass filter (Chroma, Bellows Falls, VT) and focused onto the aperture of a 50 μm optical fiber (Oz Optics, Ottawa, Canada) directly coupled to an avalanche photodiode (Perkin Elmer, Waltham, MA). A digital correlator (Flex03LQ-12, correlator.com, Bridgewater, NJ) was used to generate the autocorrelation curve.

FCS measurements were made in 8-well chambered coverglasses (Nunc, Rochester, NY) passivated by polylysine conjugated polyethylene glycol treatment to prevent αS adsorbtion to the chamber surface. Binding and aggregation studies were made by titrating 1:3 POPS/POPC vesicles into 100 nM or 50 nM αS, respectively, in Tris buffer. For each FCS measurement 25 traces of 10 seconds each were recorded and averaged together to obtain statistical variations. For the binding studies, the average curve was fit to an equation for multiple species of differing brightness (Equation 1) using MATLAB (The MathWorks, Natick, MA).

$$G(\tau) = \frac{\sum_i Q_i^2 N_i g_i}{\left(\sum_i Q_i N_i\right)^2} \qquad (1)$$

Where Q_i is the brightness of the i^{th} species relative to species 1, N_i is the number of molecules of species i in the focal volume, and g_i is the autocorrelation function of species i.

For two species (free protein and vesicle-bound protein) diffusing in three dimensions through a diffraction limited focal volume, this equation becomes[4]:

$$G(\tau) = \frac{1}{N}\left(F_F * \frac{1}{1+\frac{\tau}{\tau_{\alpha S}}} * \sqrt{\frac{1}{1+\frac{s^2\tau}{\tau_{\alpha S}}}} + Q*\left(1-F_F\right)* \frac{1}{1+\frac{\tau}{\tau_{vesicle}}} * \sqrt{\frac{1}{1+\frac{s^2\tau}{\tau_{vesicle}}}} \right) \qquad (2)$$

where *s* is the ratio of radial to axial dimensions of the focal volume, determined to be 0.2 for our system, and $\tau_{\alpha S}$ and $\tau_{vesicle}$ are the diffusion times of αS and vesicles, respectively, which were measured independently and fixed for binding measurements. $\tau_{\alpha S}$ was obtained from an αS-only solution, while the highest lipid concentration of the titration was used for $\tau_{vesicle}$ since little free protein is expected at that point. Binding measurements were fit using Equation 2. The only free parameters were N, the number of proteins, F_F, the fraction of αS free in solution, and Q, the average brightness of the vesicles relative to a single αS.

Binding curves were generated by plotting the fraction of bound protein against the concentration of accessible lipid. Two lipid concentrations were chosen from intermediate points in the binding curves, where the fraction of bound protein can be determined with highest accuracy, and molar partition coefficients K_P were calculated as described previously using Equation 3[5].

$$K_P = \frac{[\alpha S_{lipid}]}{[\alpha S_{buffer}]} = \frac{[\alpha S_{bound}] * \frac{V_{buffer}}{V_{lipid}}}{[\alpha S_{buffer}]} \qquad (3)$$

where K_P is the molar partition coefficient, αS_{lipid} is the moles of aS per volume of lipid and aS_{buffer} is the moles of free αS per volume of aqueous solution. Individual K_p values were averaged and a standard error of the mean was taken as the uncertainty. The free energy of binding is calculated as: $\Delta G = -RTln(K_P)$, where R is ideal gas constant and T is temperature.

X-ray scattering

X-ray data of oriented fluid phase lipid mixtures at 30° C were obtained at the Cornell High Energy Synchrotron Source (CHESS) using the G1 station managed by Dr. Arthur Woll. The wavelength was set with a WB_4/C multilayer monochromator to 1.1825Å, with a total beam intensity of ~10^{12} photons/sec/mm^2. Beam width was 0.26mm and the beam height was 1.2mm. The samples were ~10 μm thick along the normal due to the ~2000 bilayers. The angle of the flat samples was cycled uniformly once a second from -3 to 7 and back to -3 degrees relative to the beam during the 30-60s LAXS exposures. Data were collected using a Flicam CCD (Finger Lakes Instrumentation, Lima, NY) with a 1024x1024 pixel array with pixel size 69.78 μm/pixel. The sample-to-CCD distance was 353.7 mm for LAXS, calibrated using a silver behenate standard with D-spacing 58.4 Å. Temperature was controlled with a Neslab Controller (Portsmouth, NH) and monitored using a Cole-Parmer thermistor thermometer (Vernon Hills, IL).

The analysis of diffuse data from oriented stacks of fluctuating fluid bilayers has been previously described[6-10] and will only briefly be summarized here. The scattering intensity for a stack of oriented bilayers is the product: $I(\mathbf{q}) = S(\mathbf{q})|F(q_z)|^2/q_z$, where $\mathbf{q} = (q_r,q_z)$, $S(\mathbf{q})$ is the structure interference factor, $F(q_z)$ is the bilayer form factor and q_z^{-1} is the usual low angle approximation to the Lorentz factor for narrow oriented samples and a tall beam for which all the sample remains in the beam for all relevant q. The first step of the analysis obtains an apparent bilayer bending modulus K_C and the compression modulus B by fitting to the q_r dependence of the diffuse X-ray scattering. $|F(q_z)|^2/q_z$ is then determined by dividing I(q) by the S(q) derived from validated liquid crystal theory.

Volume determination

Stock solutions of POPS and POPC in chloroform and truncated αS (1-100AA) in hexafluoroisopropanol (HFIP) were prepared and mixed together using a repeating dispenser on a Hamilton syringe in a 200:1 lipid:protein mole ratio. Organic solvent removal was monitored by precise weighing after repeated evaporations in a vacuum oven at 50° C until no further change in weight. Lipids and lipid mixtures were hydrated as precise, dilute solutions between 0.2 and 1 weight percent in milli-Q water. Lipid molecular volume in fully hydrated MLV was determined at 30±0.01°C using an Anton-Paar USA DMA4500 (Ashland, VA) vibrating tube densimeter. Molecular volume was calculated for a sample with lipid mass m_L and water mass m_W using

$$V_L = \frac{M_L}{0.6022\rho_L}\left[1 + \frac{m_w}{m_L}\left(1 - \frac{\rho_S}{\rho_W}\right)\right], \qquad (4)$$

where M_L = molecular weight of lipid mixture, ρ_S and ρ_W are the densities of the samples and water, respectively.

Structural Analysis

The x-ray $|F(q_z)|$ data were simultaneously fit to the Scattering-length Density Profile (SDP) model that parses the lipid molecule into components whose volumes provide the underlying description[11]. The volume probabilities are first determined by the principle of volume conservation enforced by the SDP model which guarantees satisfaction of an important relation between the area A and the zeroth order form factors F(0)[12]:

$$AF(0) = 2(n_L - \rho_W V_L), \qquad (5)$$

where V_L is the measured lipid or lipid mixture volume, n_L is the number of electrons in the mixture (n_L = 428 for POPS + Na^+, 420 for POPC), and ρ_W = 0.333e/Å^3 is the electron density of water for x-rays. Volume probabilities are converted to electron density by multiplying by the number of electrons and dividing by the volume of the component group. For truncated alpha-Synuclein (100 AAs, αS), the volume was calculated to be

11,882 Å^3, and its molecular weight 10010g/mol, based on literature crystal data[13]. Volumes for POPS and POPS/αS (200:1) were also measured using the DMA densimeter. As shown in Supplemental Table S1, (V_m = volume of mixture, V_l = volume of lipid) a small, 1% lipid volume expansion occurred with 200:1 POPS/αS. The volume of the lipid mixture POPS:POPC (1:3) was nearly identical to the calculated volume of the two components in the mixture.

Supplemental Table S1.

Lipid	$X_{\alpha S}$	T (°C)	V_M (Å^3)	V_L (Å^3)
POPS	0	30	-----	1196.4 ± 3.6
POPS	0.005	30	1257.9 ± 2.6	1204.8
POPS/POPC (1:3)	0	30	-----	1244.4 ± 3.0
POPC[9]	0	30	-----	1256.5 ± 2.0
POPC	0.005	30	Undetermined	------

The molecular volume could not be determined for POPC/αS (200:1) since it decreased as a function of increasing concentration using Eqn. 1, presumably due to incomplete binding at all concentrations up to 1%.

Simulation Methods

Parameters for the Martini CGMD force field were used as previously published[14,15]. All simulation timings are reported as scaled simulation time (scaled time = 4 x simulation time) to correct for accelerated dynamics due to the CGMD force field. In order to obtain starting configurations, we first built a pure 200-lipid (100 per monolayer), POPC membrane with 22 CG waters per lipid. This system was equilibrated for 800ns at 303K. Next, we randomly selected 50 POPC (25 per monolayer) into POPS, while adding the appropriate 50 Na+ counter ions. The 200-lipid, POPS:POPC (25:75) system was subsequently minimized and equilibrated for 2μs. This system was then replicated 4x4x1 (x, y, z periodic cell replicates) to obtain the 3200-lipid system. This system was then minimized and equilibrated for 16μs and a production run of 24μs performed (40μs total). Residues 1-99 of αS (190 total CG beads) were modeled either as a contiguous extended α-helix or as a two-helix model with residue 38-44 defined as a random coil. All secondary structure constraints were applied as defined for the MARTINI force field[15]. Although αS secondary structure was constrained, the protein underwent significant bending along the helix. For the αS systems, a 400-lipid POPC system was constructed in an elongated rectangular configuration (x-lateral dimension twice y-lateral dimension) such that a single αS could span the diagonal of the periodic cell. The pure 400-lipid system was equilibrated for 800ns at 303K and a single αS was added to both monolayers, with the protein positioned proximal to the membrane, translating overlapping water molecules, generating a building block for the symmetric system. The system was equilibrated using 800ns of progressively relaxed constraints followed by 4 μs equilibration run (simulation time). The system was then replicated, 4x2x1 to generate a 3200-lipid patch with equal *xy*-dimensions. The asymmetric system was constructed from the pure 3200 lipid system with 8 αS added to the top monolayer and 184 lipids randomly removed (46 POPS and 138 POPC). Detailed compositions for each simulation are listed in Supplemental Table S2.

CGMD simulations were run using GROMACS 4 program using a leap-frog algorithm to integrate the equations of motion with an integration time step of 25 fs and coordinates recorded every 0.1 ns[16]. All simulations were run in parallel on a supercomputer cluster with dual Quad-core CPUs per node, with systems prepared in the isothermal-isobaric (NPT) ensemble at constant pressure and temperature (1 bar and 303 K respectively). A Nose´-Hoover thermostat[17,18] with a time constant of 2.5 ps was used to control the ensemble

temperature, while an analog Parrinello-Rahman barostat[19,20] with a time constant of 250 ps was used to keep the pressure fixed. The lipids, protein, ions and the water were coupled to independent thermostats to avoid unwanted heating/cooling artifacts. Pressure coupling was applied as semi-isotropic resulting in a tensionless bilayer. We utilize the convention of describing the effective time sampled as a four-fold increase over the simulation time, due to a "smoothing" of the energy profile in coarse grain simulation[14]. All production simulations were run a minimum of 40 μs (scaled simulation time).

Protein Depth via Coarse-Grained Molecular Dynamics

Both the PMF and unconstrained simulations were focused on a small system comprised of a single αS at a 1:400 protein to lipid ratio (using 3:1 POPC:POPS).

Although these simulations are not directly comparable to the experimental systems (different protein-lipid ratio and configuration), the reduction in complexity was necessary to reduce the degrees of freedom and allowing for an adequate sampling at every PMF data point.

Potential of Mean Force

The potential of mean force (PMF) describes the energy landscape along a specific reaction coordinate. For this study we explored the partitioning of αS as a function of the center of mass (COM) of αS relative to the bilayer normal axis (*z*-dimension). The PMF was determined using umbrella sampling on a system with a single αS interacting with a 400-lipid (3:1 POPC:POPS) symmetric bilayer, and 8800 coarse-grained waters. The reaction coordinate sampled between -5.0 to 35.0Å relative to the bilayer COM in 1.0Å increments, requiring 40 separate simulations with a total scaled simulation time of 160 μs. Initial configurations were built by pulling the single αS with constraints applied to the lipid headgroup in the z-dimension to reduce bilayer deformation. An initial equilibration simulation of 400 ns was run with strong protein and weak headgroup constraints to relax the system, followed by 400 ns of production simulation with a harmonic potential applied to constrain the COM of the protein at the specific reaction coordinate ($Z_{\alpha S}$) with a force constant of 1000 kJ mol^{-1} nm^{-2}, following the approach by Monticelli et al[15]. The resulting PMF (see Supplemental Figure S9A) was determined using the *g_wham* algorithm in GROMACS[21].

Unconstrained Simulations

A brute force MD approach employing multiple different αS starting configurations (6 total with $Z_{\alpha S}$ = 0, 8, 13, 16, 20, and 25Å) were simulated and analyzed to compare the $Z_{\alpha S}$ trajectories. Each system was started from an "constrained-equilibrated" state, where an initial 400 ns simulation was performed with harmonic constraints applied to both the protein's position as well as the lipid headgroups to establish starting configurations. All constraints were relaxed and removed over 100 ns, and each system simulated for an additional 4 μs using the same simulation parameters as earlier productions runs. Comparison of protein partitioning depth relative to the bilayer COM illustrated rapid convergence within the first 160 ns of unconstrained simulation (see Supplemental Figure S9B).

Data Analysis

Trajectories were manipulated and processed using the GROMACS v.4.5.3 simulation package. All subsequent data analysis was performed using MATLAB (7.9.1:R2009b, Service Pack 1) with the signal processing toolbox.

Surface Rendering and Curvature Determination

Monolayer height functions were obtained using the Real-space Interpolation method as detailed in References 21 and 22[2,22]. Briefly, surfaces were defined by the PO_4 lipid headgroup beads, using a Monge representation,

$z = h(x, y)$. An ideal low-pass filter with crossover wavenumber, q_0 = 1.5 nm^{-1}, was used to isolate the undulation modes. Both monolayer and undulation reference surface (URS) surfaces were obtained from the corresponding filtered spectra, using a real-space grid of ~0.3 nm resolution. Distance measurements (D_{pp}, D_{hh}, Number densities) were corrected using the undulation correction method[2].

The height surface, time-correlation function was defined as

$$C(x, y, \tau) = \frac{1}{T}\int_0^{\tau} h(x, y, t)h(x, y, t - \tau)d\tau, \qquad (6)$$

and the relaxation time τ_h, is determined for each *xy*-node by

$$h(x, y, \tau_h) \stackrel{\text{def}}{=} C(x, y, \tau) = \frac{1}{e}. \qquad (7)$$

where n_{xy} is the number of *xy*-nodes (100x100).

Curvature was defined following the formalism of Brown et al., the mean and Gaussian curvature (κ_m, κ_g) were defined as follows, with principle curvatures (κ_1, κ_2) defined as $\left(\kappa_1 \stackrel{\text{def}}{=} \frac{1}{R_1}\right)$ and where $h_x \stackrel{\text{def}}{=} \frac{\partial h}{\partial x}$ [23].

$$\kappa_m = \frac{(\kappa_1 + \kappa_2)}{2} = \frac{(1 + h_x^2)h_{yy} + \left(1 + h_y^2\right)h_{xx} - h_x h_y {h_{xy}}^2}{\left(1 + h_x^2 + h_y^2\right)^{3/2}}, \qquad (8)$$

$$\kappa_g = \kappa_1\kappa_2 = \frac{h_{xx}h_{yy} - {h_{xy}}^2}{\left(1 + h_x^2 + h_y^2\right)^2}. \qquad (9)$$

All partial derivatives were defined using a centered finite difference method applied to the filtered membrane surfaces (i.e. the URS and both monolayer surfaces). Once both κ_m and κ_g were determined, the principle curvatures were found solving the quadratic equation

$$\kappa_1^2 - 2\kappa_m\kappa_1 + \kappa_g = 0. \qquad (10)$$

Resulting in

$$\kappa_1 = \kappa_m + \sqrt{\kappa_m^2 - \kappa_g} \qquad (11)$$

and

$$\kappa_2 = \kappa_m - \sqrt{\kappa_m^2 - \kappa_g} \quad . \qquad (12)$$

The two different measures of local protein effects (residue profiles and local average-surface) were determined as follows. Residue profiles were interpolations of each surface quantity (height, mean curvature, and Gaussian curvature) for every protein's residue *xy*-coordinates. These values were averaged across all proteins for a given monolayer ($n_{protein}$ = 8) and over all time frames in the production run (n_{frames} = 6000). For the symmetrically distributed protein system, each monolayer was treated separately, and for the bottom monolayer, the sign of the mean curvature was inverted, when applicable, for direct comparison to the top leaflet and the asymmetric system.

The local averaged-surface representation is determined via a rotational transformation, resulting in each protein's backbone *xy*-coordinates to be aligned in a common coordinate system. The residues $n_{res} = [n_2(x,y), \cdots, n_{50}(x,y), \cdots, n_{98}(x,y)]$ were used to define the helical backbone and were linearly fit to determining the angle θ, defined between the fitted line and the periodic cell x-axis. The new *xy*-coordinates $h(x', y')$ were then determined by the multiplying the original coordinates with a rotation matrix defined about the *z*-axis, such that

$$[x' \quad y'] = \begin{bmatrix} \cos\theta & -\sin\theta \\ \sin\theta & \cos\theta \end{bmatrix} [x \quad y] \ . \tag{13}$$

After rotation, residue HIS_{50} is set to the new origin, N-terminus is positioned at a minimum *x*-value, and *C*-terminus at a maximal *x*-value. Surfaces are then both spatially averaged (for each protein in the monolayer) and temporally averaged over all time steps analyzed.

Full References:

(25) Cooper, A. A.; Gitler, A. D.; Cashikar, A.; Haynes, C. M.; Hill, K. J.; Bhullar, B.; Liu, K. N.; Xu, K. X.; Strathearn, K. E.; Liu, F.; Cao, S. S.; Caldwell, K. A.; Caldwell, G. A.; Marsischky, G.; Kolod-ner, R. D.; LaBaer, J.; Rochet, J. C.; Bonini, N. M.; Lindquist, S. Science 2006, 313, 324.

(27) Nakamura, K.; Nemani, V. M.; Azarbal, F.; Skibinski, G.; Levy, J. M.; Egami, K.; Munishkina, L.; Zhang, J.; Gardner, B.; Waka-bayashi, J.; Sesaki, H.; Cheng, Y.; Finkbeiner, S.; Nussbaum, R. L.; Masliah, E.; Edwards, R. H. J Biol Chem 2011, 286, 20710.

(58) Takamori, S.; Holt, M.; Stenius, K.; Lemke, E. A.; Gronborg, M.; Riedel, D.; Urlaub, H.; Schenck, S.; Brugger, B.; Ringler, P.; Muller, S. A.; Rammner, B.; Grater, F.; Hub, J. S.; De Groot, B. L.; Mieskes, G.; Moriyama, Y.; Klingauf, J.; Grubmuller, H.; Heuser, J.; Wieland, F.; Jahn, R. Cell 2006, 127, 831.

(60) Garcia-Reitbock, P.; Anichtchik, O.; Bellucci, A.; Iovino, M.; Ballini, C.; Fineberg, E.; Ghetti, B.; Della Corte, L.; Spano, P.; Tofaris, G. K.; Goedert, M.; Spillantini, M. G. *Brain* **2010**, *133*, 2032.

Supplemental Table S2. CGMD system composition.

System	# POPC	# POPS	# Water	# Na^+	# Cl^-	# αS	Total Beads
Pure	2400	800	70400	800	0	0	112800
Symmetric αS	2400	800	70400	976	240	16	116256
Asymmetric αS	2262	754	70400	842	120	8	112090
Single αS	2382	794	70400	805	15	1	112698

Supplemental Table S3. Structural parameters from CGMD simulation. Simulation results are presented for both continuous and broken-helix protein conformations. D_{PP} describes the bilayer thickness, whereas ΔD_{PP} is the change in thickness relative to the pure system. A_{UC} describes the area per unit cell (defined by the undulating area per lipids per monolayer^2). $Z_{\alpha S}$ presents the mean and standard deviation of the protein number density, describing the depth of partitioning of the protein into the bilayer.

System	D_{PP} [Å]	ΔD_{PP} [Å]	A_{UC} [Å^2]	$Z_{\alpha S}$ [Å]
Pure	42.7	-	63.2	-
Symmetric-Continuous	41.8	-0.9	67.6	17.5 ± 4.3
Symmetric-Broken	41.3	-1.4	68.3	17.2 ± 4.4
Asymmetric-Continuous	42.1	-0.6	66.2	17.4 ± 4.6
Asymmetric-Broken	42.3	-0.4	66.1	17.5 ± 4.9

Supporting Figures

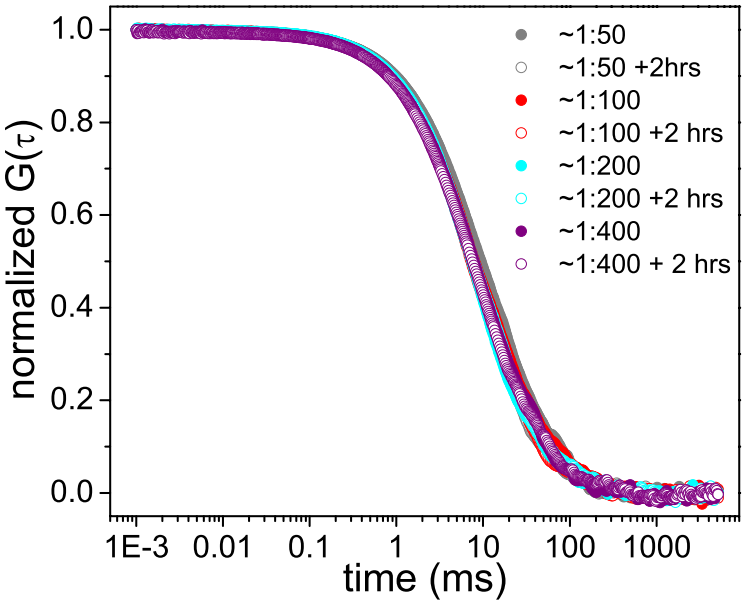

Supplemental Figure S1. Assessing the aggregation of αS(residues 1-100). Normalized autocorrelation curves for a range of αS:lipid ratios overlay very nicely, indicating that the binding interaction is stable and suggesting no evidence of aggregation over the course of 2 hours. The conditions were 50 nM αS 1-100 (S9C for labeling) with 1:3 POPS:POPC LUVs in water, at various protein: lipid ratios (from ~1:50-1:400) at time=0 and time=2 hrs. Aggregation would result in an erratic, increased lag in the autocorrelation curve as we have previously shown with the protein tau[2].

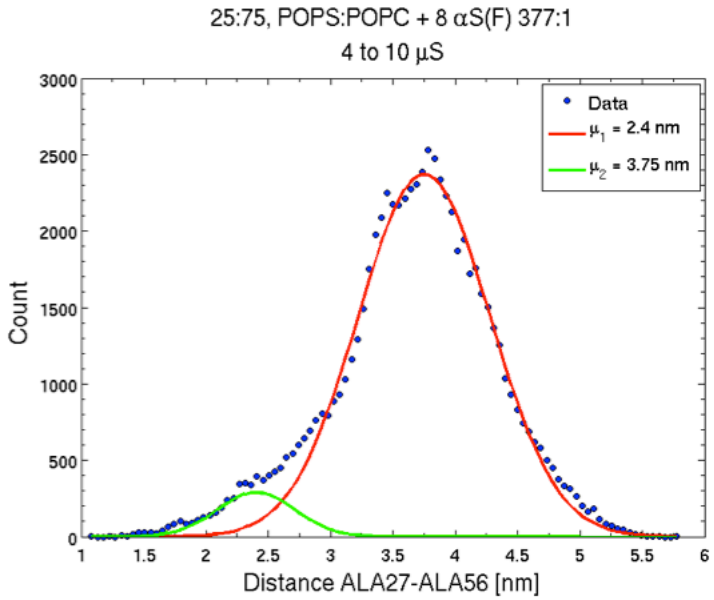

Supplemental Figure S2. ALA27-ALA56 distance distributions take for all proteins (8 in total) in the asymmetric broken-helix simulation. μ_1 and μ_2 detail the respective means of the 2-Gaussian fit of the simulated distance distribution (*blue circles*).

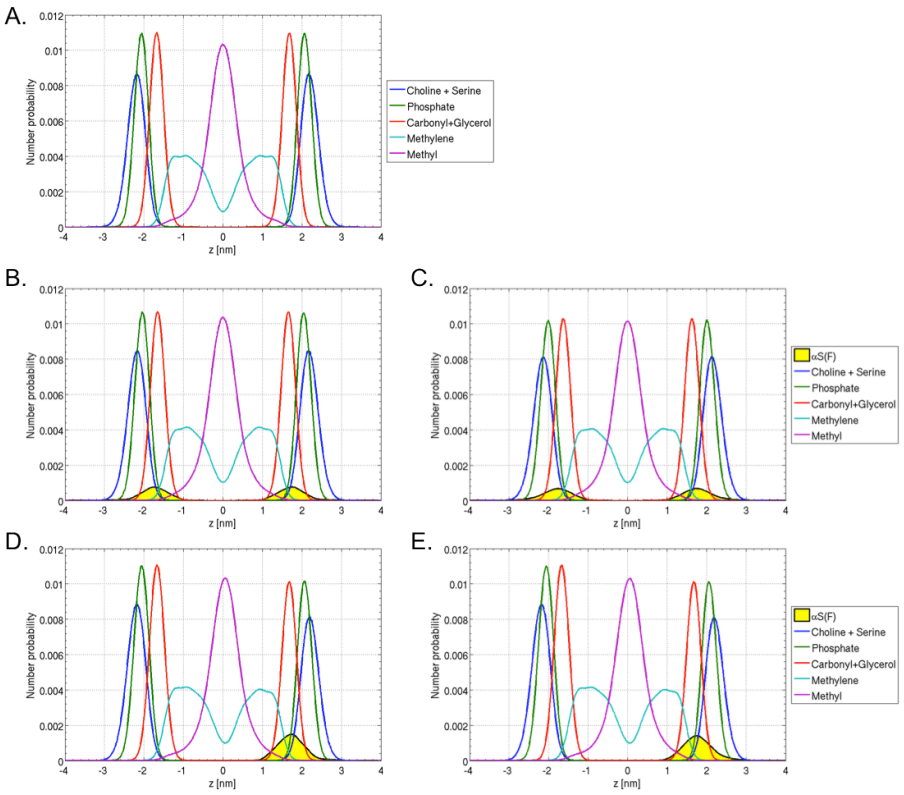

Supplemental Figure S3. Normalized component number probabilities determined from CGMD simulations. (A) Pure, (B) Symmetric-Continuous, (C), Symmetric-Broken, (D) Asymmetric-Continuous, and (E) Asymmetric- Broken. In each system the αS partitions between the Phosphate and Carbonyl-Glycerol distributions.

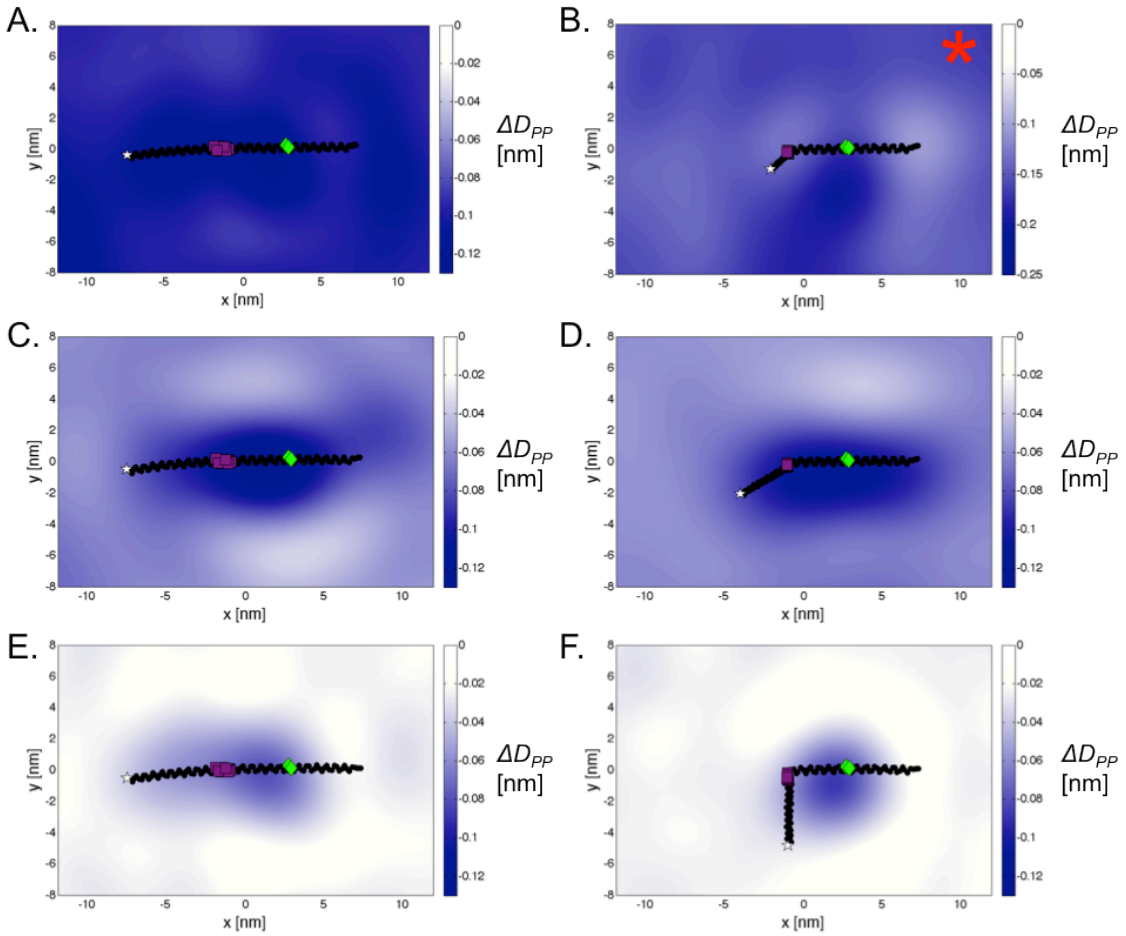

Supplemental Figure S4: ΔD_{PP} profiles for (A) Symmetric-Continuous, (B), Symmetric-Broken, (C) Asymmetric-Continuous, (D) Asymmetric-Broken, (E) Single-Continuous, and (F) Single-Broken systems with the time- and protein-averaged position of the protein in black (*white star* indicates N-terminus, *purple square* indicates linker region, *green diamond* indicates GLY67-GLY68). All systems except the symmetric-flexible show increased thinning near the protein. The symmetric-flexible system has a different color-scale, as the thinning effects were greater than observed in all other systems. In the symmetric-flexible system, the protein in the top and bottom leaflet segregated into an unregistered conformation (minimal overlap of protein across the membrane), leading to a bilayer with two regions of locally increased protein concentration, therefore behaving as an asymmetric system in those areas, changing the intrinsic curvature-field.

* = Change of color-scale.

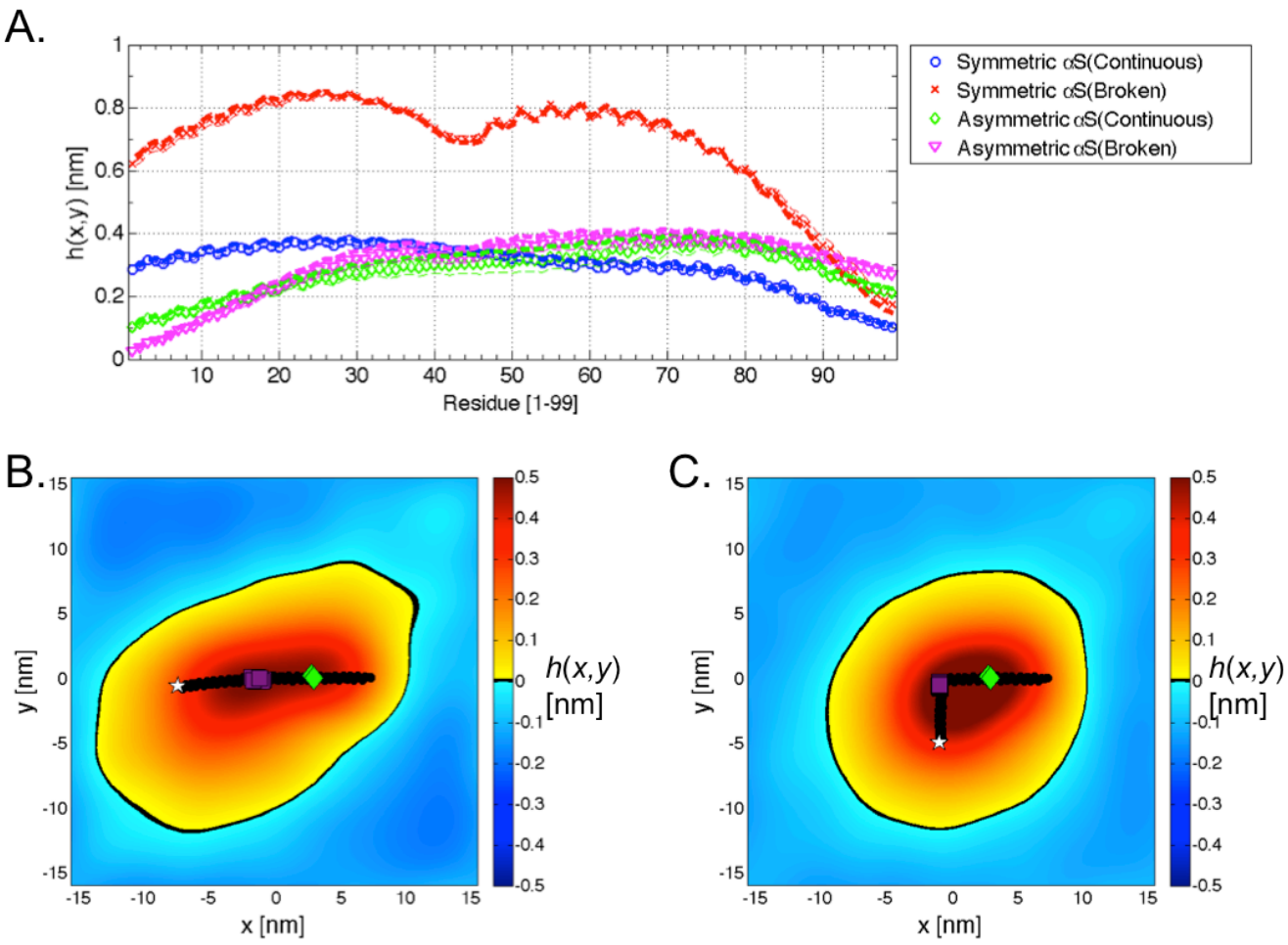

Supplemental Figure S5. Protein stabilized height surfaces. (A) Comparisons of time- and protein- averaged height surface intensity, h(x,y)=z, at the average αS residue position showing preference for positive deflections in the undulation reference surface. Time-averaged undulation reference surface for (B) Single-Continuous and (C) Single-Broken αS systems. Both B and C show the stabilization of a membrane 'bulge' proximal to the protein in *black* (*white star* indicates N-terminus, *purple square* indicates linker region, *green diamond* indicates GLY67-GLY68).

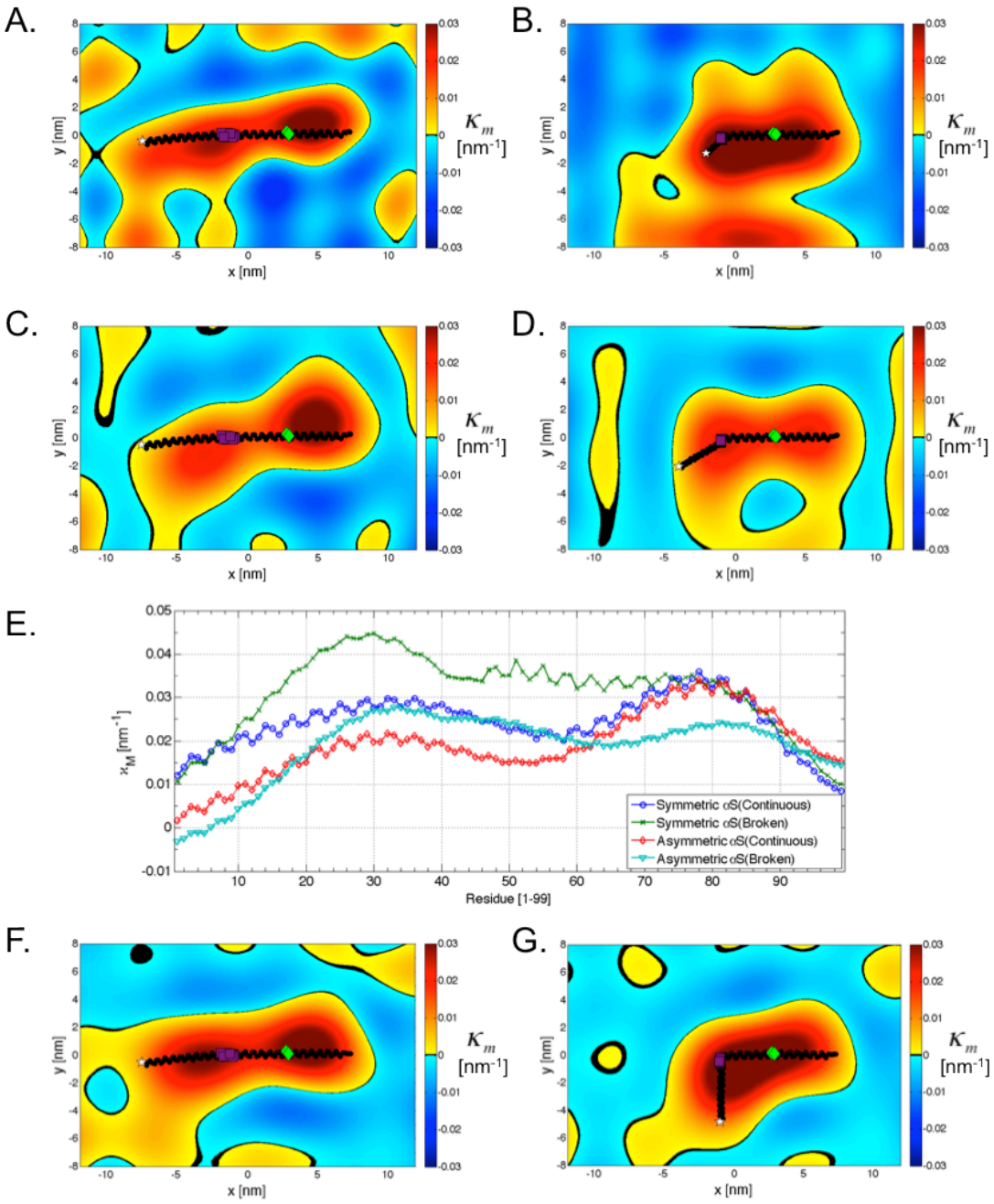

Supplemental Figure S6. Time- and Protein-averaged mean curvature-field (κ_m). Panels A and B correspond to the symmetric protein system, (A) continuous and (B) broken-helix conformations. Both panels present averages over protein in the top(outer) leaflet as the effect for either monolayer is indistinguishable. Time- and protein-averaged mean curvature for the asymmetric system (C) continuous and (D) broken-helix conformations. (E) κ_m defined along the protein helical backbone for each system showing a global preference for positive mean curvature at the protein. Panels F and G present the mean curvature-field for the single protein systems, continuous and broken-helix respectively. All curvature-fields were averaged over 6000 frames, with 8 proteins per frame for the symmetric and asymmetric systems, using the re-orientation method described in Data Analysis. For all curvature-field panels, color-scale units are [nm^{-1}]; protein is in *black, white star* indicates N-terminus, *purple square* indicates linker region, *green diamond* indicates GLY67-GLY68.

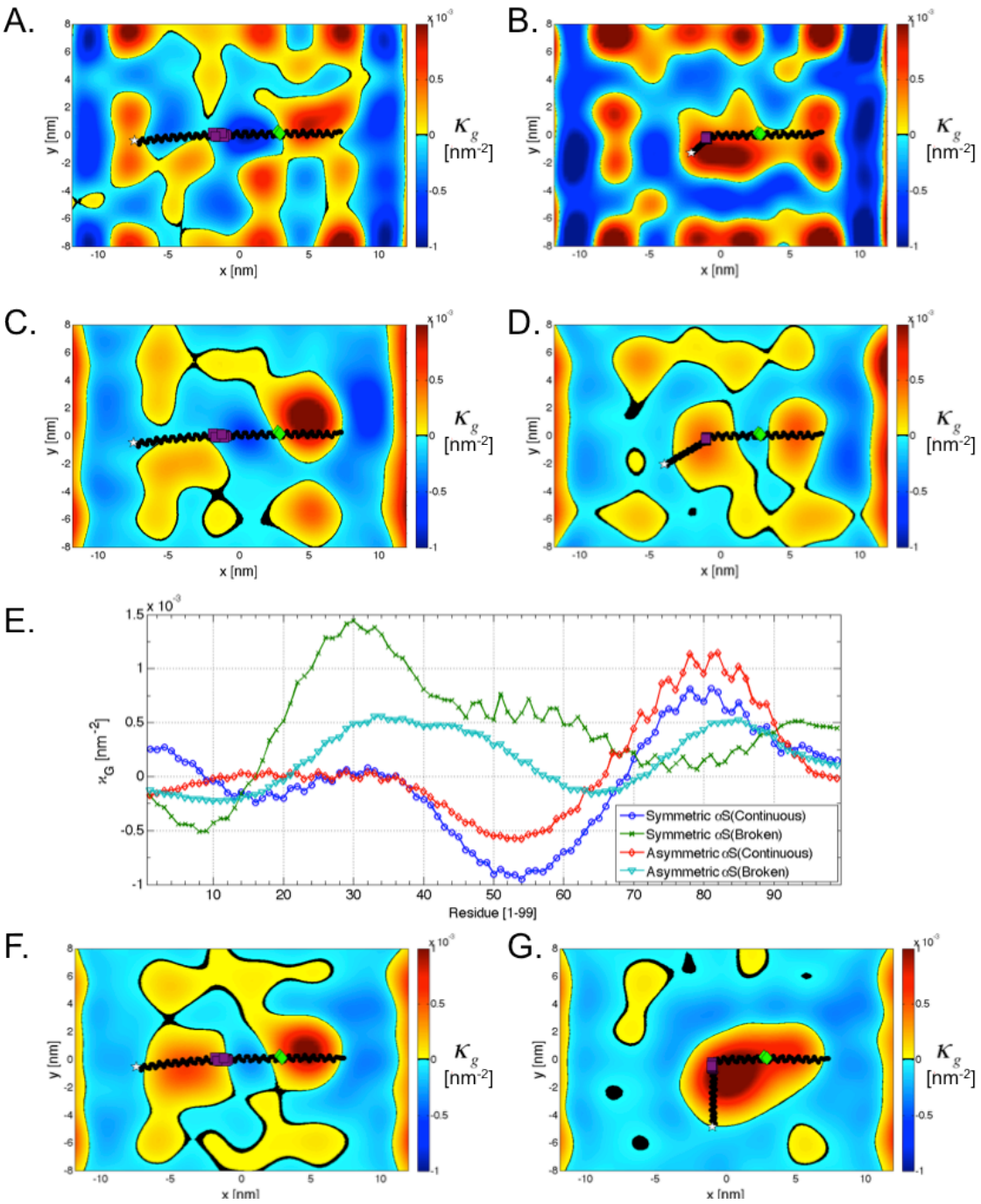

Supplemental Figure S7. Time- and Protein- averaged Gaussian curvature-field (κ_g). Panels A and B correspond to the symmetric protein system, (A) continuous and (B) broken-helix conformations. Both panels present averages over each protein in the top(outer) leaflet as the effect for either monolayer is indistinguishable. Time- and protein-averaged Gaussian curvature-fields for the asymmetric protein system (C) continuous and (D) broken-helix conformations. (E) κ_g defined along the protein helical backbone for each system (except symmetric-broken) showing a transition to negative Gaussian curvature near the GLY67-GLY68 position of the protein, an area known for increased flexibility. Panels F and G present the Gaussian curvature-field for the single protein systems, continuous and broken-helix respectively. All curvature-fields were averaged over 6000 frames, with 8 proteins per frame for the symmetric and asymmetric systems, using the re-orientation method described in Data Analysis. For all curvature-field panels, color-scale units are [nm^{-2}]; protein is in *black, white star* indicates N-terminus, *purple square* indicates linker region, *green diamond* indicate GLY67-GLY68.

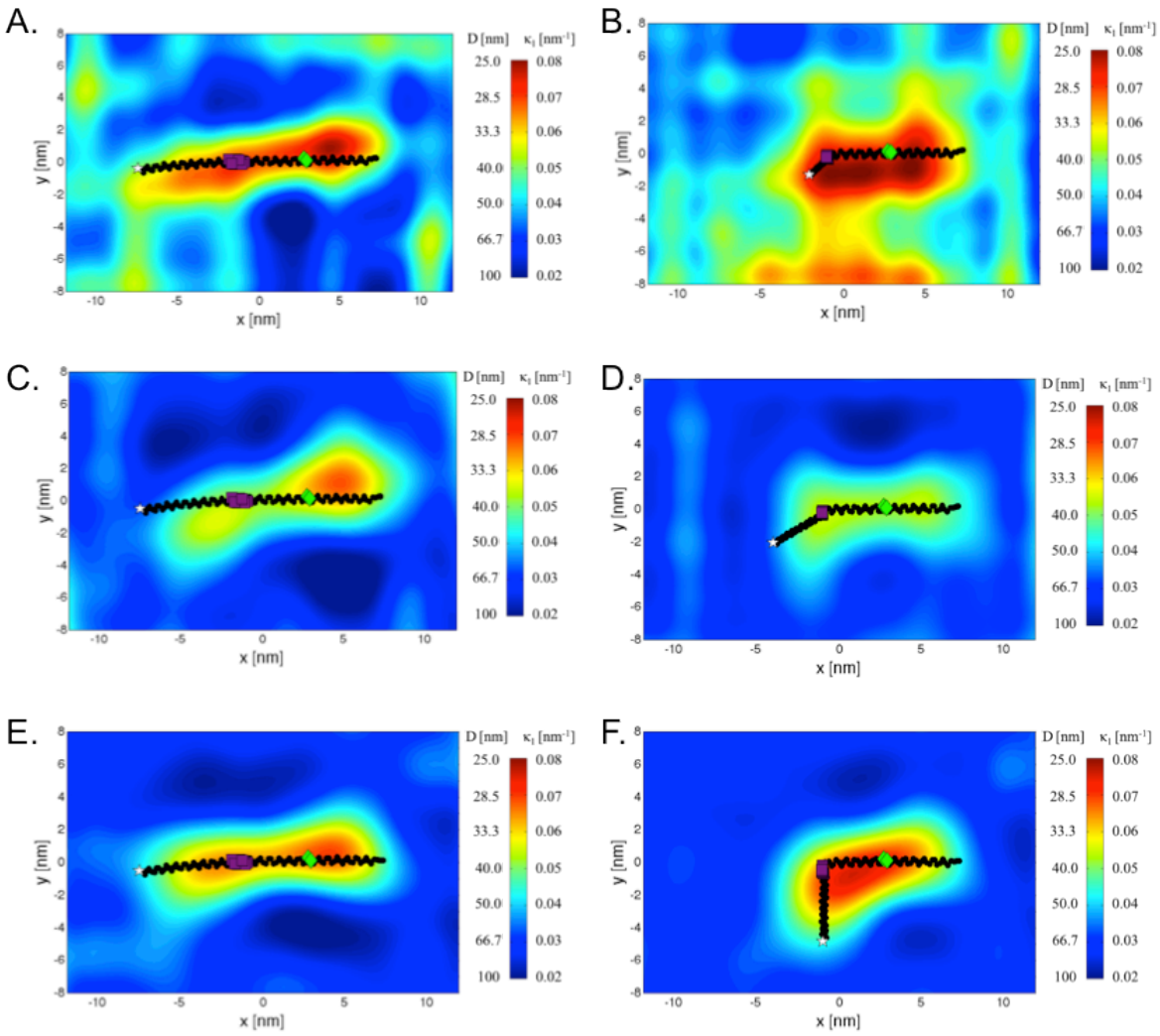

Supplemental Figure S8. Maximum Principle curvature-field (κ_1). Time- and protein-averaged maximum principle curvature fields provide a measure of the curvature in a spherical vesicle-like environment for (A) Symmetric-Continuous, (B) Symmetric-Broken, (C) Asymmetric-Continuous, (D) Asymmetric-Broken, (E) Single-Continuous, and (F) Single-Broken systems. For all curvature-field panels, color-scale units are [nm^{-1}] with the corresponding vesicle diameter in [nm], $D = 2/\kappa_1$; protein is in *black, white star* indicates N-terminus, *purple square* indicates linker region, *green diamond* indicates GLY67-GLY68.

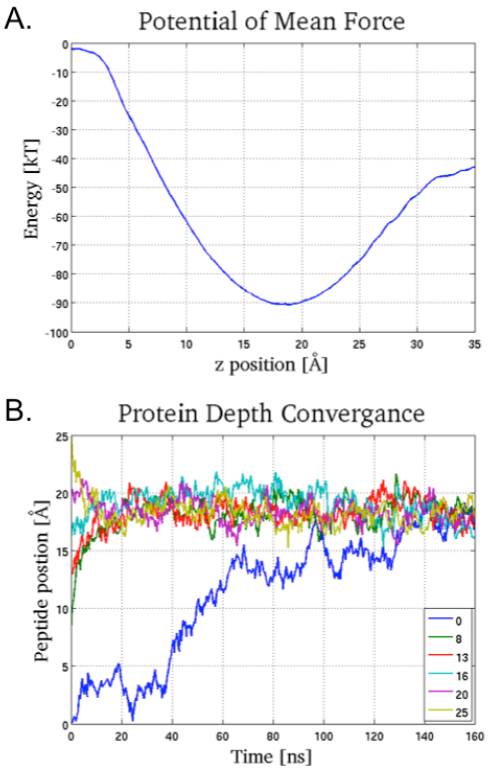

Supplemental Figure S9. αS partitioning explored via Coarse-Grained MD . (A) Potential of Mean Force (PMF) for αS, determined using the z-position of the protein's center of mass as the reaction coordinate, illustrates peripherally bound protein, consistent with previous EPR results[1]. (B) Brute force MD using multiple protein-starting configurations shows rapid convergence to a peripherally bound protein position, consistent to the PMF result.

References (Supporting Information)

(1) Jao, C. C.; Der-Sarkissian, A.; Chen, J.; Langen, R. *Proceedings of the National Academy of Sciences* **2004**, *101*, 8331.
(2) Braun, A. R.; Brandt, E. G.; Edholm, O.; Nagle, J. F.; Sachs, J. N. *Biophys J* **2011**, *100*, 2112.
(3) Trexler, A. J.; Rhoades, E. *Biochemistry* **2009**, *48*, 2304.
(4) Rauer, B.; Neumann, E.; Widengren, J.; Rigler, R. *Biophysical Chemistry* **1996**, *58*, 3.
(5) Middleton, E. R.; Rhoades, E. *Biophys. J.* **2010**, *99*, 2279.
(6) Lyatskaya, Y.; Liu, Y. F.; Tristram-Nagle, S.; Katsaras, J.; Nagle, J. F. *Phys Rev E* **2001**, *63*, 0119071.
(7) Liu, Y. F.; Nagle, J. F. *Phys Rev E* **2004**, *69*, 040901.
(8) Kučerka, N.; Liu, Y. F.; Chu, N. J.; Petrache, H. I.; Tristram-Nagle, S. T.; Nagle, J. F. *Biophys J* **2005**, *88*, 2626.
(9) Kučerka, N.; Tristram-Nagle, S.; Nagle, J. F. *Biophys J* **2006**, *90*, L83.
(10) Zemel, A.; Ben-Shaul, A.; May, S. *Journal of Physical Chemistry B* **2008**, *112*, 6988.
(11) Kucerka, N.; Nagle, J. F.; Sachs, J. N.; Feller, S. E.; Pencer, J.; Jackson, A.; Katsaras, J. *Biophys J* **2008**, *95*, 2356.
(12) Nagle, J. F.; Wiener, M. C. *Biophys J* **1989**, *55*, 309.
(13) WEBsite **2010**.
(14) Marrink, S. J.; Risselada, H. J.; Yefimov, S.; Tieleman, D. P.; de Vries, A. H. *Journal of Physical Chemistry B* **2007**, *111*, 7812.
(15) Monticelli, L.; Kandasamv, S. K.; Periole, X.; Larson, R. G.; Tieleman, D. P.; Marrink, S. J. *Journal of Chemical Theory and Computation* **2008**, *4*.
(16) Hess, B.; Kutzner, C.; van der Spoel, D.; Lindahl, E. *Journal of Chemical Theory and Computation* **2008**, *4*, 435.
(17) Nose´, S. *Mol. Phys.* **1984**, *52*, 255.
(18) Hoover, W. G. *Physical Review A* **1985**, *31*, 1695.
(19) Parrinello, M.; Rahman, A. *J. Appl. Phys.* **1981**, *52*, 7182.
(20) Nose´, S.; Klein, M. L. *Mol. Phys.* **1983**, *50*, 1055.
(21) Hub, J. S.; De Groot, B. L.; Van der Spoel, D. *Journal of Chemical Theory and Computation* **2010**, *6*, 3713.
(22) Brandt, E. G.; Braun, A. R.; Sachs, J. N.; Nagle, J. F.; Edholm, O. *Biophys J* **2011**, *100*, 2104.
(23) Brown, F. L. *Annu Rev Phys Chem* **2008**, *59*, 685.